42th AIAA Plasmadynamics and Lasers Conference AIAA-2011-3277
27 – 30 Jun 2011, Honolulu, HI

Aero Optics of Subsonic Boundary Layers over Backward Steps

Adam E. Smith[1], Stanislav Gordeyev[2], and Eric Jumper[3]
University of Notre Dame, Notre Dame, Indiana, 46545

An experimental study of the two-dimensional transition from turbulent boundary layer over small backward-facing steps is presented in order to investigate the effect of the separation bubble behind the back-step on the aero-optical environment, as well as to demonstrate the capacity for characterizing complex flow fields using non-intrusive optical measurement techniques such as the Malley Probe. The flow field surrounding backward facing step is characterized using hot-wire anemometry, wall pressure measurements, and the Malley Probe. These measurements are presented for two step heights, and the results are discussed in details. The development of the sub-shear layer is observed behind the step, along with increased levels of OPD_{rms} within the separated region. After re-attachment, an eventual recovery of the boundary layer is observed, although aero-optical levels recover to higher than pre-step levels. A simple model to account for step effects on boundary layers downstream of the back-step is proposed. Also, a relative contribution from the near-wall region of the boundary layer to overall levels of the aero-optical distortions was estimated.

I. Introduction

THE study of the aero-optic problem is chiefly concerned with the propagation of optical wavefronts through turbulent flow fields found in the environments in which airborne optical systems operate [1]. When a wavefront passes through media of unsteady variable density, and therefore variable index-of-refraction, the result is an unsteady, non-uniform aberrations imposed on the original wavefront. These deviations in the near-field environment surrounding an aircraft may cause severe degradation in optical signal quality within any system which seeks to make use of such a signal. Two particular turbulent flows of interest in the study of this problem are compressible boundary layers and free-shear layers.

There has been much work done in the characterization of the optically-aberrating effects of high-speed, turbulent boundary layers. Cress, et al. [2,3] have investigated the relationship between aero-optical measurements in zero-pressure-gradient flows and several non-optical flow characterization quantities including Mach number, boundary layer displacement thickness, elevation angle, and wall heating. Scaling relationships for the OPD_{rms} were developed and shown to be consistent with experimental data. Additionally, Cress, et al. [2,4] have shown that within this type of flow, the most optically-active structures inside the boundary layer typically convect at approximately 0.8 of the freestream velocity, suggesting that the most optically active structure exists in the outer region of the boundary layer.

Through the Gladstone-Dale constant, K_{GD}, the density and index of refraction are related:

$$n(\boldsymbol{x},t) - 1 = K_{GD}\,\rho(\boldsymbol{x},t). \tag{1}$$

Given a refractive index field, the level of optical distortions is described as the optical path length, OPL,

$$OPL(\boldsymbol{x},t) = \int_{s1}^{s2} n(\boldsymbol{x},t)ds. \tag{2}$$

although the deviation from the spatially-averaged OPL, or optical path difference (OPD), is typically used,

[1] Graduate Student, Department of Mechanical and Aerospace Engineering, Hessert Laboratory for Aerospace Research, Notre Dame, IN 46556, Student Member.
[2] Research Associate Professor, Department of Mechanical and Aerospace Engineering, Hessert Laboratory for Aerospace Research, Notre Dame, IN 46556, Senior AIAA Member.
[3] Professor, Department of Mechanical and Aerospace Engineering, Hessert Laboratory for Aerospace Research, Notre Dame, IN 46556, AIAA Fellow.

$$OPD(\boldsymbol{x},t) = OPL(\boldsymbol{x},t) - \overline{OPL}(\boldsymbol{x},t) \tag{3}$$

where the overbar denotes the spatial average. The Malley Probe [5] can be used to measure OPD as a function of time at locations in the flow field of interest by measuring a time history of deflection jitter angle, $\phi(x,t)$ and a local convective speed, U_C, to compute OPD,

$$OPD(x,t) = -U_c \int_0^t \phi(x,t)dt \tag{4}$$

In some practical applications, the boundary layer develops over the wall with small slope or surface discontinuities. In this paper we will consider the effect of a small, less than the boundary-layer thickness, back-step on the aero-optical performance of the flow after the back-step. The backward-step flow has been widely investigated as an experimental geometry which provides a well-defined region of separation for both laminar and turbulent flows, as well as its simplicity in modeling surface features which are often encountered in real engineering fluid flows. The relationships between extent of these separation regions and various flow parameters for the backward step have been studied extensively. Following early work on the backward step by a number of researchers, Armaly, et al [6] performed a thorough study of the locations and sizes of separation regions as a function of Reynolds number with values spanning the transitional range between laminar and fully turbulent incoming flow. Results showed additional regions of separation present for transitional Reynolds numbers which ceased to appear once the transition to the turbulent regime occurred, and that the average reattachment location appears to become independent of Reynolds number in the fully-turbulent regime.

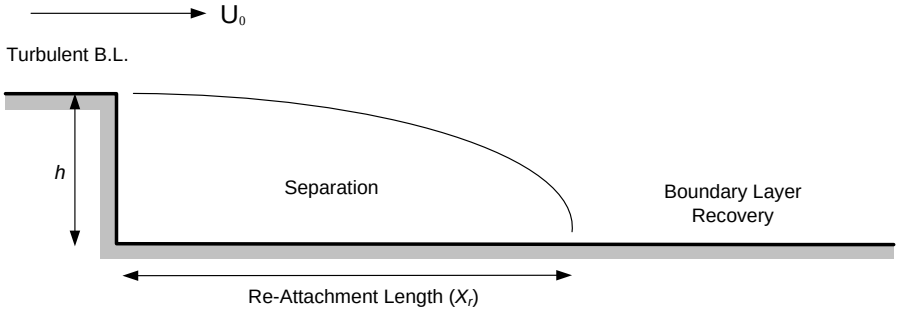

Figure 1: Schematic of backward-step flow regimes.

Experiments investigating the flow in the recovery region have demonstrated that at streamwise locations as far as 50 step heights, the mean flow does not fully recover to its initial state. However, log-law velocity profile recovery was demonstrated at various locations within that interval [7]. Extensive studies by Morris and Foss [8] identified a number of distinct flow regions that compose the whole transitional flow field from the turbulent boundary layer to a single-stream layer. Their results demonstrate that in the near-step region the outer section of the turbulent boundary layer profile is unaffected, and they extensively quantified the development of the sub-shear layer and the free shear layer. While this paper focuses on small step heights, the results from [8] were found to be relevant to the development of the sub-shear layer in the near-step region. Small backward steps have also been of interest due to their role as significant noise sources. Minsuk and Wang [9] have performed computational studies of flows over small steps, exploring the effects of step height on sound generation. Recently Siegel, et al. [10,11] have also used the Malley Probe to investigate the development of large scale structures within the single-stream shear layer created by the large backward step.

This paper investigates the aero-optical changes in the boundary layer due to a small, on the order of $0.1-0.2\delta$, backward-facing step. The objective was to investigate the flow behavior in the separation and the re-attachment region to see, in particular, how long it would take for the boundary layer to go back to its "undistorted" behavior. An optical analysis of the near-region immediately after boundary-layer separation, the formation of the sub-shear layer, the re-attachment, and the recovery regions was performed in order to characterize the aero-optical effects of the flow separation phenomenon in comparison to the incoming canonical turbulent boundary layer.

II. Experimental Setup & Data Reduction

Experimental measurements of the boundary layer over the backward step were conducted in a wind tunnel at the Hessert Laboratory for Aerospace Research at the University of Notre Dame. Wind tunnel velocity was manipulated by controlling the speed of vacuum pumps, as well as with a pressure bleed valve installed in the plenum. Two step heights, 3 mm and 6 mm, or approximately 10%-20% of the incoming boundary layer thickness, were tested at Mach number 0.4. As shown in Figure 1, the wind tunnel has an open circuit design with a 150:1 inlet contraction ratio, followed by a boundary layer development section, a boundary layer measurement section, and a measurement section downstream of backward step. The cross-section of the boundary layer development and measurement sections is 9.9 cm by 10.1cm, and the total length is 195 cm to the location of the backward step. Freestream velocity was measured using total and static pressure ports mounted upstream of the back-step on the side wall, see Figure 2.

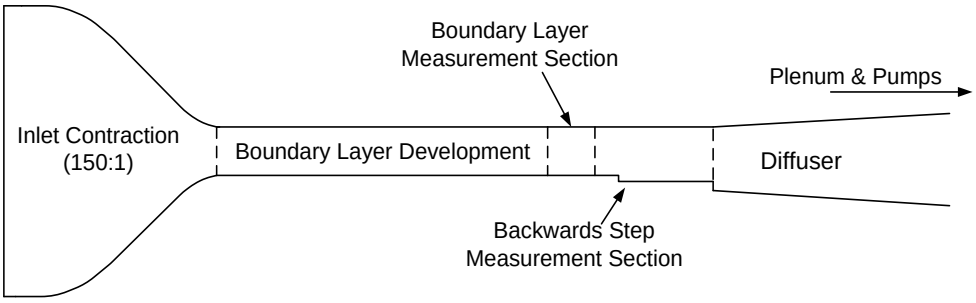

Figure 2: Side view of transonic boundary layer test facility at Notre Dame, with backward-step measurement geometry installed (*Not to scale*).

To create the back-step, the location of bottom wall was modified such that the measurement cross section expands to 9.9 cm by (10.1 + h) cm, where h is the step height. The streamwise length of this expanded section is 49.5 cm, and the entire length of the boundary layer development and back-step measurement sections are constructed of clear Plexiglas to allow for optical access. A schematic of the backward-step measurement section is shown in Figure 3. Several variants of the test section's upper and lower walls were constructed to allow access for both optical and hot-wire anemometry measurements while preserving the designed test section dimensions.

Spatial coordinates are defined such that the streamwise direction, x, is zero at the step location with positive values of x increasing in the direction of the flow. The vertical coordinate, y, starts from zero at the floor of the boundary layer development section and increases vertically across the test section.

Static pressure ports were installed along the side walls of the test section before and after the step in order to monitor variations in the mean pressure in the streamwise flow direction. Static pressure measurements were taken using three Setra differential pressure transducers, with two transducers measuring the values of the upstream static and total pressure, and the third taking single point measurements at a specific downstream wall static port. For each measurement location, 2.5×10^5 samples were obtained and averaged to compute the corresponding mean static pressure. The pressure coefficients for compressible flow along the test section calculated by

$$c_p = \frac{2}{\gamma M_\infty^2}\left(\frac{p}{p_\infty} - 1\right). \tag{5}$$

Hot-wire velocity measurements were obtained with a single hot-wire using a commercial constant temperature anemometer with a built-in low pass filter, with a sampling rate of 100 kHz and a low-pass filter cutoff of 50 kHz. The hot-wire was mounted downstream of the backward step via a two-degree of freedom traverse system; the hot-wire was calibrated in the freestream for Mach numbers ranging from M = 0.16 to 0.43. Incoming boundary layer profiles were measured upstream of the step at the testing Mach number M = 0.4, and both the incoming displacement thickness

$$\delta_o^* = \int_0^\infty \left(1 - \frac{U(z)}{U_\infty}\right) dz, \tag{6a}$$

and the incoming momentum thickness

$$\theta_o = \int_0^\infty \frac{U(z)}{U_\infty}\left(1 - \frac{U(z)}{U_\infty}\right) dz \tag{6b}$$

were computed and it was found that $\delta_o^* = 3.19$ mm and $\theta_o = 2.50$ mm for the incoming boundary layer, giving Re_θ = 20,000. Clauser's method was used with to calculate the wall friction velocity, $U_\tau = 4.89$ m/s.

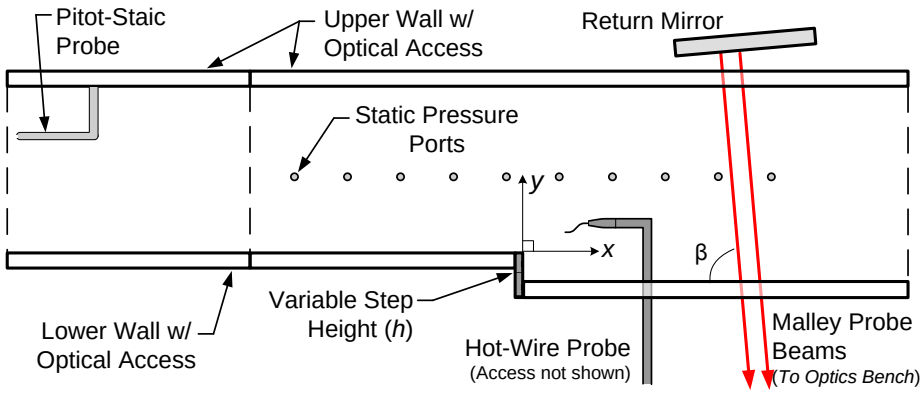

Figure 3: Schematic of the backward-step measurement section, with instrumentation shown.

Optical measurements were performed using the Malley Probe similar to the design reported by Gordeyev, et al [5]. The spacing of the beams shown in Figure 3 was set at 4.5 mm and their diameter was approximately 0.5 mm. Beams were propagated at an elevation angle, β, defined in Figure 3, of 68° in order to obtain clean optical data in the near-step region. Beam deflection angles, or jitter data, $\phi(t)$, were collected at a number of streamwise positions at a sampling frequency of 200 kHz. Amplitude spectra of the jitter signal or aero-optical spectra, $\hat{\phi}(f)$, were computed for each of the analyzed streamwise locations. From this data, values of OPD_{rms} were then calculated as a function of streamwise location using the Fourier-version of the Eq. (4),

$$OPD_{rms}^2 = 2U_c^2 \int_0^\infty \frac{|\phi(f)|^2}{(2\pi f)^2} df. \tag{7}$$

Spectral contamination from both-low frequency mechanical vibrations and high-frequency electronic noise were removed in the post-processing calculation of OPD_{rms}. This was accomplished through a combination of low-pass filtering in post-processing, and placing bounds of integration in the frequency domain between 600 Hz to 70 kHz. Aero-optical spectra were scaled using the relationship proposed by Wittich at el. [12] for turbulent, subsonic, compressible boundary layers,

$$\hat{\phi}_{\text{norm}}(St(\delta^*)) = \frac{\hat{\phi}(f)}{\frac{\rho}{\rho_{SL}} \frac{\delta^*}{U_\infty \sin\beta} M^2}, \tag{8}$$

where ρ_{SL} is the sea-level density, and the Strouhal number is defined as $St(\delta^*) = (f\delta^*/U_\infty)/\sin(\beta)$.

III. Results

To characterize the hydrodynamic environment in the near-step region, velocity profiles for the back-step size of h = 3.0 mm were collected shortly upstream of the back-step and at one-millimeter intervals from 1 mm to 10 mm downstream of the back-step. The scaled near-step velocity and velocity RMS contours are shown in Figure 4. All spatial coordinated are normalized by the incoming momentum thickness, θ_0.

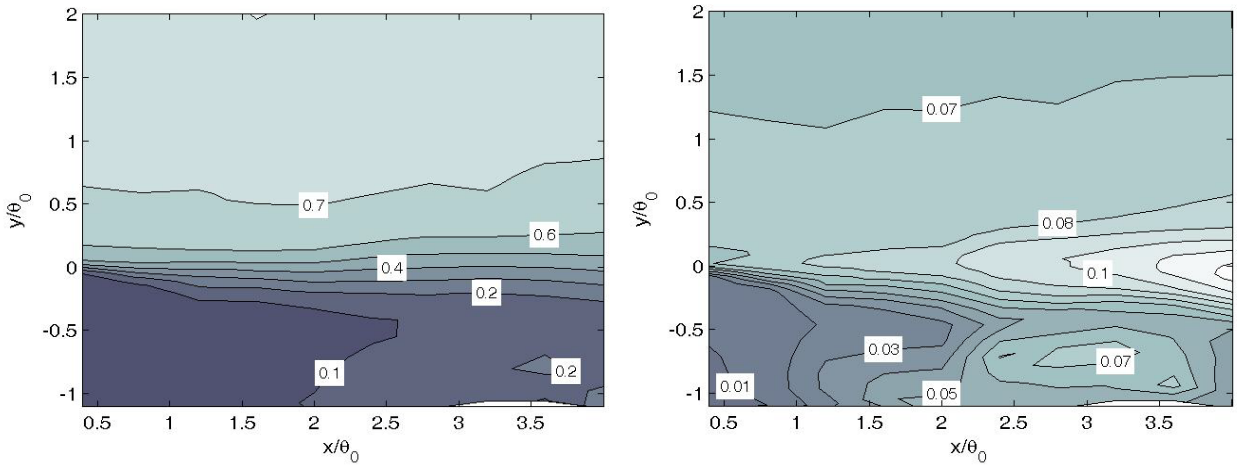

Figure 4: Contours of (a) U/U_∞ and (b) U_{rms}/U_∞ in the near-step region for h = 3 mm.

For values of $x/\theta_0 > 1$, the spread of the velocity contours and the increase in velocity RMS values indicates the appearance and the growth of a sub-shear layer. This observation was further supported by the investigation of evolution of the maximum velocity derivative du/dy in the streamwise direction. The near-step velocity-derivative data is plotted in Figure 5 along with the experimental fit from [8] for the single-stream shear layer. In the region up to $x/\theta_0 \approx 3$ there is good agreement with the fit from their experimental data for the sub-shear layer region.

In addition to the velocity data, the aero-optical environment around the backward-facing step was characterized at number of streamwise locations using the Malley Probe. Measurements in the near-step, the re-attachment, and the recovery regions were acquired for both h = 3.0 and 6.0 mm steps. Figure 6 shows the evolution of the aero-optical spectra $\hat{\phi}(f)$ at several locations downstream of the step. As the distance from the step increases, a peak emerges from the high-frequency end of the boundary-layer spectra; with the increasing streamwise distance from the back-step the location of the frequency peak, f_m, decreases and the maximum amplitude $\hat{\phi}(f_m)$ increases. This trend in growth continues until approximately 5 step heights in the streamwise direction, at which point the growth of the amplitude spectra stops. For streamwise locations greater than 5h, the peak amplitude of $\hat{\phi}(f)$ decreases as flow re-attaches and begins to recover back to the undisturbed boundary layer. We will consider these flow regions separately.

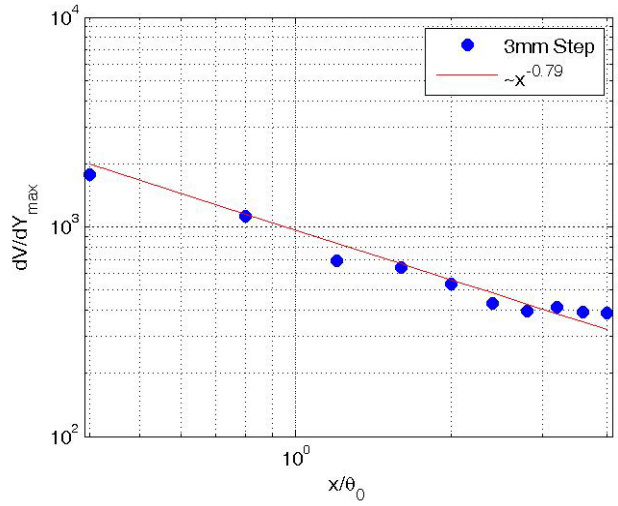

Figure 5: Maximum velocity derivative development with comparison to results from [8].

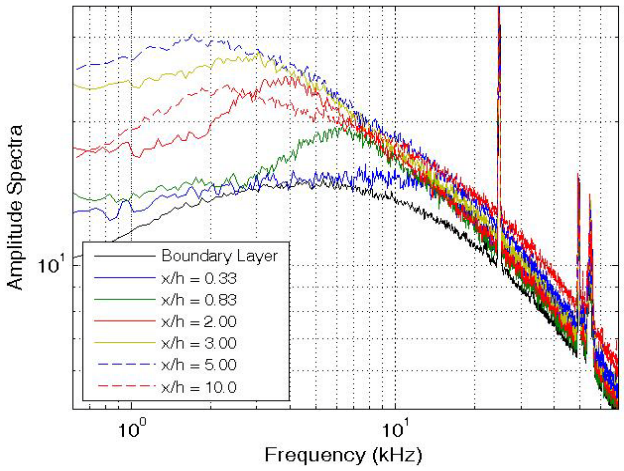

Figure 6: Aero-optical spectra at different streamwise locations for h = 6 mm.

Near-Step Region

Normalizing the aero-optical spectra in the near-region of the flow immediately downstream of the back-step by the peak amplitude and location, as shown in Figure 7, a self-similarity was observed in the this region for streamwise locations between 1.2 to $3.6\theta_0$ for the 3-mm step, and between 1.2 to $7.2\theta_0$ for the 6-mm step. The observation provides further evidence of the presence of self-similar the sub-shear layer.

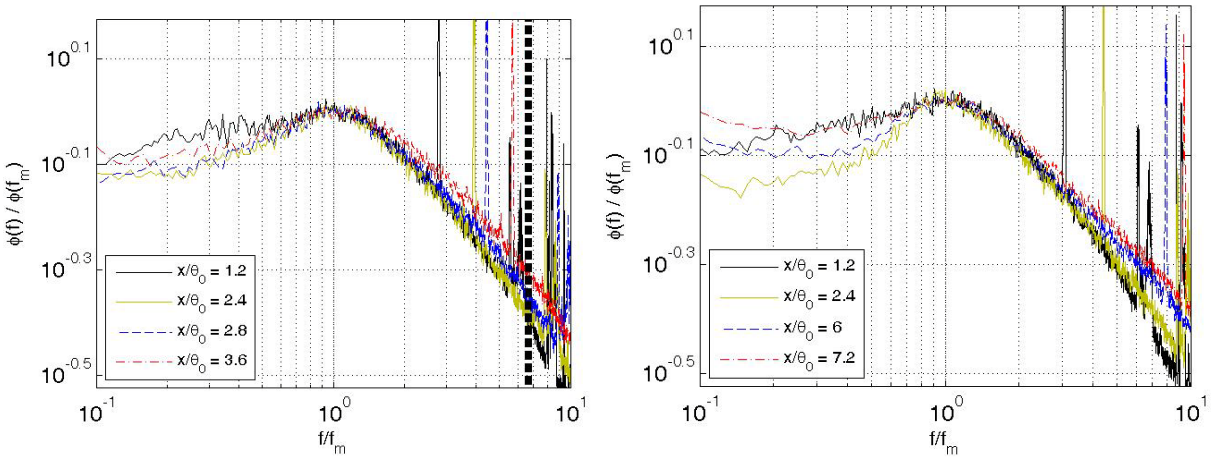

Figure 7: Scaled $\widehat{\phi}(f_m)$ for (left plot) 3 mm step and (right plot) 6 mm step.

In addition to the evidence for the sub-shear layer's presence from velocity measurements and the spectral self-similarity scaling in the near-step region, comparisons of the streamwise evolution of the aero-optical spectrum peak, f_m, and OPD_{rms} also provide additional information on the sub-shear-layer development. The location of the peak, $f_m(x)$ is calculated from the amplitude spectra at each streamwise location. The results for both step heights, normalized by the incoming momentum thickness are shown in Figure 8. Also in this Figure the experimentally-obtained fit for the maximum frequency for the sub-shear layer from [8], $St_{\theta_0} \sim (x/\theta_0)^{-0.71}$, is plotted for comparison. The dominant frequency peak related to the sub-shear layer extracted from aero-optical spectra correlates well with the sub-layer in the single shear-layer experiment [8] for streamwise locations between $1.2\theta_0$ and $6\theta_0$ for the 3-mm step and up to $10\theta_0$ for the 6-mm step. The main difference between the flow over the back-step and the flow in the single-stream shear layer is the presence of the re-circulation region for the first one. These results suggest that the evolution of the sub-shear layer in the near region downstream of the back-step is primarily governed by the local inflection-instability mechanism and only weakly depends on the global topology of the separation region.

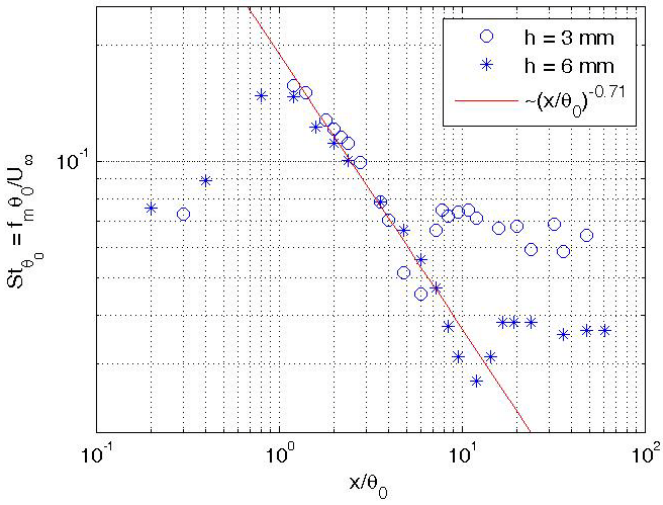

Figure 8: Maximum frequency (f_m) development with sub-shear layer fit from [8].

In addition to the aero-optical spectra and the peak-frequency data, the streamwise evolution of OPD_{rms} for two step heights was computed using Eq. 7. In Figure 9, OPD_{rms} appeared to increase linearly with the streamwise distance at similar rates for both step heights. The streamwise extent of this linear growth period is also consistent with previous observations from f_m-data. However, after this initial region, the OPD_{rms} reached a maximum value and started decreasing farther downstream. The peak value in OPD_{rms} and its streamwise location were increasing with the step height. All these observations support the idea that in the near-step region the emerging sub-shear layer becomes optically significant; the initial growth of the sub-shear layer was found to be independent of the step height and the streamwise extend the sub-shear layer was a function of the step height.

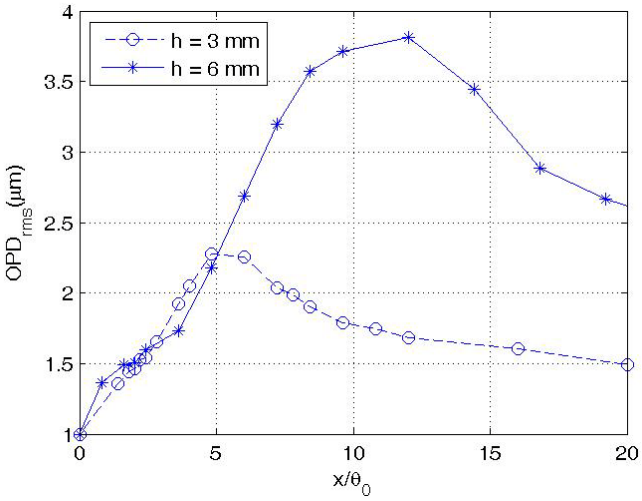

Figure 9: OPD_{rms} development in the separation region.

Re-attaching and recovery regions

Inspection the aero-optical spectra for streamwise locations beyond the near-region, *x/h* > 2, showed that at approximately 5-6 step heights downstream from the step the peak of the spectrum stops increasing with the streamwise distance, and starts decreasing in amplitude; also, there is a distinct increase in the high-frequency end of the spectra for the streamwise locations *x/h* between 2 and 7, as can be seen in Figure 10. The streamwise location at which the spectrum peak stops increasing, is consistent with the re-attachment location reported by other authors [6,7]. So, this shape-changing trend in the spectra suggests that the separated flow is been re-attached and the mean velocity profile is changed from the shear-layer-like to the boundary-layer-like profile.

After the aero-optical spectra begin decreasing in amplitude for the streamwise locations x/h > 5, the spectra begin to exhibit a similarity to turbulent boundary-layer spectra, but with greater amplitudes. This observation and the observations of other researchers [7] indicates that after flow is re-attached, velocity profiles and turbulence levels do not recover back to the boundary-layer upstream of the back-step and it takes the re-attached flow significant distances downstream of the step to relax back to the canonical boundary layer. In order to compare aero-optical spectra in the recovery region to the undistorted boundary layer upstream of the back-step, we normalized the aero-optical spectra by the amplitude of the spectrum peak.

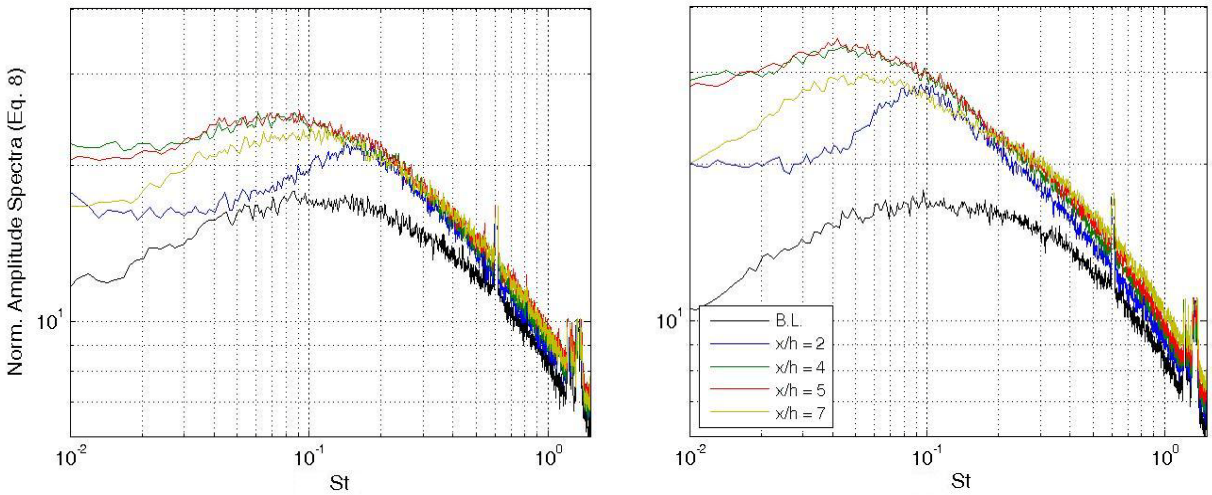

Figure 10: Scaled aero-optical spectra for the (left plot) 3-mm step and (right plot) 6-mm step in the separation and re-attachment regions.

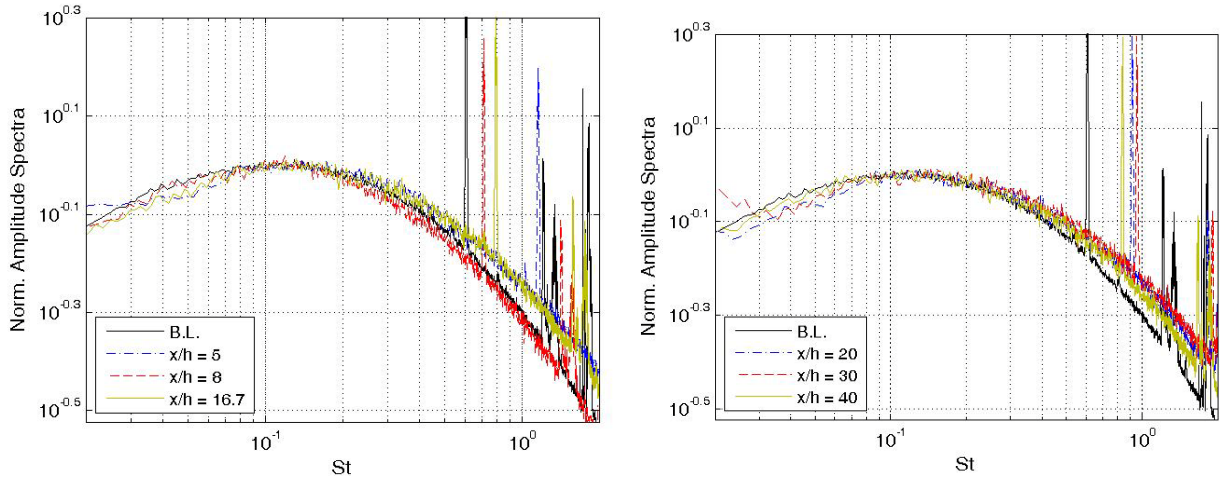

Figure 11: Revised scaling of aero-optical spectra in the recovery region for h = 3mm.

Normalized plots of the spectra in the re-attachment and the recovery regions are shown in Figure 11. The similarity with the incoming boundary layer is achieved only for the streamwise distances of approximately x/h=20, except for the energy in the high-frequency end of the spectra, St > 0.2, where the amount of aero-optical energy is still higher compared to the undistorted boundary-layer energy. One possible reason of the effect is the separation region creates the sub-shear layer and therefore higher level of turbulence near the wall and this turbulent energy continues to dissipate into higher-frequency range via the energy-transfer mechanism.

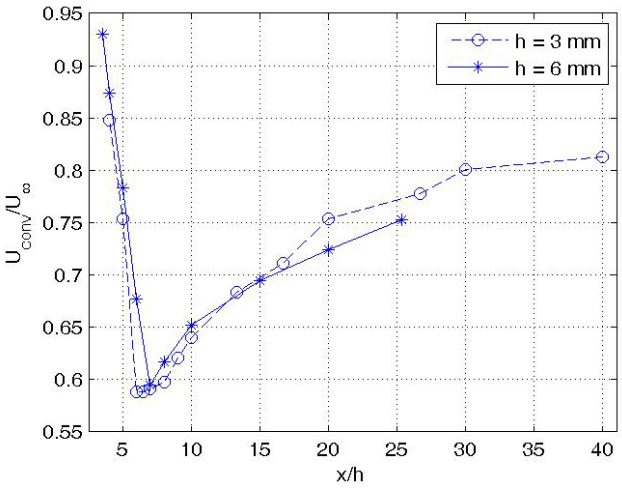

Figure 12: Variation of the local convective velocity in streamwise direction.

The measurements of the local convective speed as a function of the distance from the back-step are presented in Figure 12. The convective speed of aero-optical structures of the canonical boundary layer is approximately 0.8 of the freestream speed. The sub-shear layer is located in the low-speed portion of the boundary layer, see Figure 4. The convective speed of the sub-shear-layer vortical structures is approximately a half-sum of the high-speed and the low-speed regions on both sides of the sub-shear layer. Assuming that the high-speed region is 0.8 of the freestream speed and the low-speed region is approximately zero, the convective speed of the aero-optical structures in the sub-shear layer would be approximately 0.4 of the freestream speed. As the Malley probe measured a weighed sum of the convective speeds from the boundary layer and the sub-shear layer, as the sub-shear layer grows stronger, the local normalized convective speed would be close to 0.4 than to 0.8, this is indeed the case in Figure 12 for the streamwise locations between x/h = 1 and 7. At x/h=7 the separated flow re-attaches, so the shear-layer started to

disappear, so the convective speed begins to approach the boundary-layer values of 0.8. By x/h~30, the results for the convective speed also suggest that the boundary layer is relaxed to its undistorted value.

Analyzing the streamwise variation of OPD_{rms} for different step heights, it was found that the results collapse for the following quantity,

$$\frac{\Delta OPD_{rms}(x,h)}{\mathrm{h}} = f(\frac{x}{h}) \tag{9}$$

where $\Delta OPD_{rms}(x,h) = OPD_{rms}(x,h) - OPD_{rms}(x=0)$. Results of the proposed scaling of OPD_{rms} are presented in Figure 13. This scaling is consistent this the previously-described evolution of the aero-optical structures in separation bubble, as the size and the strength of the sub-shear layer is proportional to the separation-bubble length, which in turn is proportional to the back-step size; therefore, the increase in OPD_{rms} after the back-step compared to the canonical boundary layer should be proportional to the step height. The peak value of OPDrms occurred at x/h ~ 5 with the value of $\Delta OPD_{rms} / h \approx 7\text{x}10^{-6}$, or, normalized to the OPD_{rms}-value for the undistorted boundary layer, $\Delta OPD_{rms} / OPD_{rms}(x=0) \approx 2.8h/\delta_0^*$. Thus, even for small steps, the added level of the aero-optical distortions can be on the order of the undistorted level. After the flow is re-attached, the value of OPD_{rms} starts decreasing and in the region range $20 < x/h < 40$, the value of OPD_{rms} asymptotes, but to a positive value of $2.6\text{x}10^{-6}$, suggesting that the flow in this region has recovered to the boundary layer state with consistently higher levels of optical aberrations when compared to the boundary layer before the step.

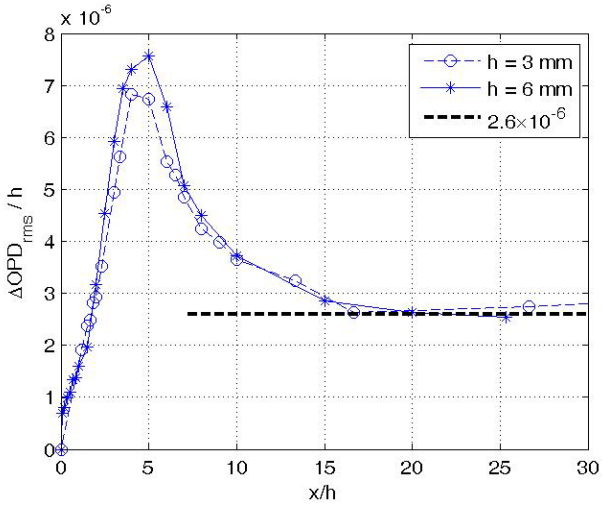

Figure 13: Streamwise evolution of OPD_{rms} in the re-attachment and the recovery regions.

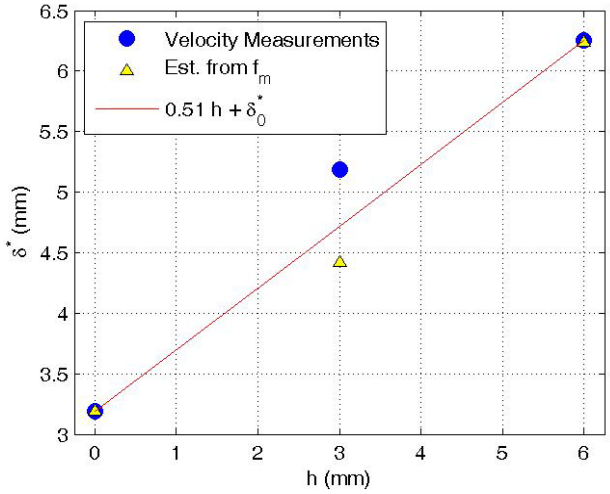

Figure 14: Values of displacement thickness in the boundary layer recovery region $x/h \cong 26$.

In [2] it was found that for turbulent, compressible subsonic boundary layers,

$$OPD_{rms}(h=0) = A\frac{\rho}{\rho_{SL}}M^2\delta_0^* \tag{10}$$

where $A = 1.7(\pm 0.2) \times 10^{-5}$. Let's assume that the recovered boundary layer can be approximates by the same expression, but with the different displacement thickness. δ^*. Substituting (10) into (9) and using the asymptote value of $2.6\text{x}10^{-6}$ for *f(x/h)*, the resulting level of OPDrms in the recovery region sufficiently downstream of the backward step can be estimated as,

$$OPD_{rms}(x,h) = A\frac{\rho}{\rho_{SL}}M^2\delta^* = OPD_{rms}(x=0) + 2.6\cdot 10^{-6}h = A\frac{\rho}{\rho_{SL}}M^2(\delta_0^* + \sigma h) \tag{11}$$

where $\delta^* = \delta_0^* + \sigma h$ and $\sigma = \frac{2.6\cdot 10^{-6}}{A\frac{\rho}{\rho_{SL}}M^2} = 1.0$.

In the region where the boundary layer spectra became self-similar, the local displacement thickness can be independently estimated assuming that the Strouhal number based on the local displacement thickness is the same as for the incoming undistorted boundary layer, similar to the procedure used to estimate the boundary-layer thickness from aero-optical spectra in [13],

$$St(\delta^*) = St(\delta_0^*) = 0.1 \text{ or } \delta^* = 0.1U_\infty/f_m \quad (12)$$

Using the values of the peak locations for both step heights at streamwise locations greater than $20h$, the calculated displacement thickness were plotted as a function the step height and results are presented in Figure 14. Direct measurements of the displacements thickness from the velocity profiles are also plotted for comparison. Both hydro-dynamical and non-intrusive aero-optical results agree with each other very well. A linear fit to the data gives the following expression for the displacement thickness, $\delta^* = \delta_0^* + 0.5h$, which also confirms that for the recovering boundary layer, the displacement thickness is proportional to step height.

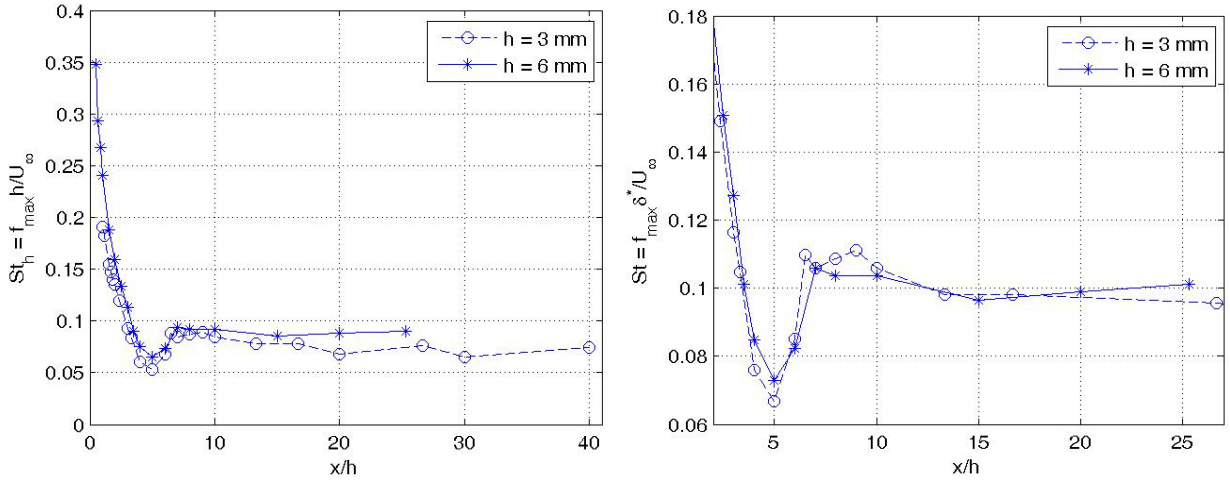

Figure 15: Peak frequency location (f_m) scaled with (a) step height h and (b) the displacement thickness δ^*.

Both estimations of the local displacement thickness, from the amplitude of the aero-optical distortions and from the location of the peak gave a linear relation versus the back-step height, although with two different constants of the proportionality. Analysis of the velocity profiles at *x/h* = 40 showed that the fluctuating velocity component is still larger compared to the undistorted values, implying that the boundary layer had not relaxed to the undistorted state yet. Also, the spatial growth and, consequentially a higher level of the aero-optical distortions of the upper boundary layers were not factored into the OPD_{rms} calculations. These reasons are most probably responsible for a higher value of the constant from the analysis of the OPD_{rms}-amplitude. In [13] the peak-location procedure was also found to be more robust and less-sensitive to experimental error in estimating the local displacement thickness. Therefore, the level of the optical-distortions in the boundary layer at subsonic speeds sufficiently downstream of the back-step was estimated to be,

$$OPD_{rms}(h) \approx 1.7 \cdot 10^{-5} \frac{\rho}{\rho_{SL}} M^2(\delta_0^* + 0.5h) \quad (13)$$

Finally, the streamwise evolution of the spectra peak normalized by both the step height and the displacement thickness in the recovery region are presented in Figure 15. For both step heights there is a sharp transition in the rate of change of f_m in the separation and the re-attachment region up to $10h$ past the step; within the separation and re-attachment regions f_m scales with *h*. Beyond re-attachment point, the spectra peak appears to scale with the displacement thickness in the recovery region, approaching to the value for the undistorted boundary layer of 0.1.

Effect of Small-Scale Structures

By modifying the near-wall region, which includes both the viscous sub-layer and the portion of the log-linear region of the canonical boundary layer and analyzing the velocity-modification effect on the aero-optical spectra at the same streamwise locations, it is possible, at least qualitatively, to bound the amount of aero-optical energy within this near-wall region. Velocity RMS profiles and aero-optical spectra at several locations in the near-step region are shown in Figure 16 (a) and Figure 16 (b), respectively. At the streamwise location of x/θ_0 = 0.4, the fluctuating-velocity profile in the near-wall region between y^+ = 0 and 60 was affected by the wall-absence and the aero-optical spectrum deviated from the canonical-boundary-layer spectrum at frequencies larger than 10 kHz. At the locations x/θ_0 = 0.8 and 1.2, the u_{rms}- profiles deviated from the canonical-boundary-layer profile in the larger near-wall region between y^+ = 0 and 200, with the corresponding change in the aero-optical spectra for frequencies

higher than 5 kHz. Assuming that all aero-optical aberrations at high-frequencies, which defined by the frequency region above the cut-off frequency, f_{cut}, is originated in the corresponding near-wall region, amount of the optical energy in this high-frequency region,

$$OPD^2_{rms}(HF) = 2U_C^2 \int_{f_{cut}}^{\infty} \frac{|\phi(f)|^2}{(2\pi f)^2} df \tag{14}$$

can be estimated by integrating the aero-optical spectrum over the range of frequencies.

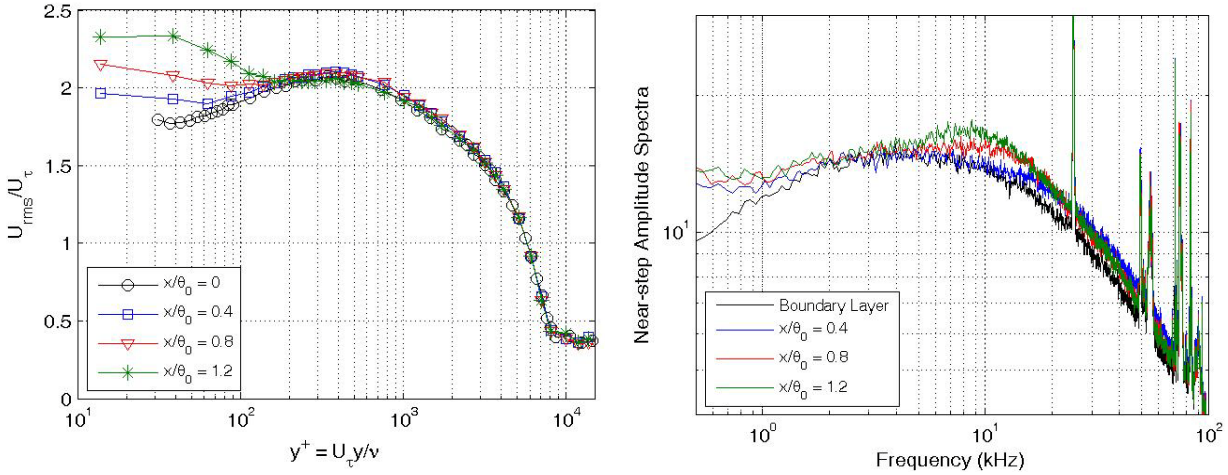

Figure 16: (a) Velocity RMS profiles in wall units and (b) amplitude of aero-optical spectra at several streamwise locations in the near-step region.

Results for the high-frequency aero-optical energy, normalized by the total aero-optical energy, OPD^2_{rms}, versus different cut-off frequencies are presented in Figure 17. For the x/θ_0 = 0.4, the cut-off frequency was 5 kHz and the amount of aero-optical energy within the near-wall region between 0 and 60 wall-units can be estimated from Figure 17 as approximately 5%. Similar calculations for the locations x/θ_0 = 0.8 and 1.2 gave an estimation of the aero-optical energy of 13% in the near-wall region below y^+ = 200. Of course, these results should be treated with caution, as several critical assumptions had been made for these estimations. Still, these results strongly suggest that the near-wall region contributes only few percent of the total level of aero-optical aberrations and the most of the aero-optical distortions are located in the outer part of the boundary layer.

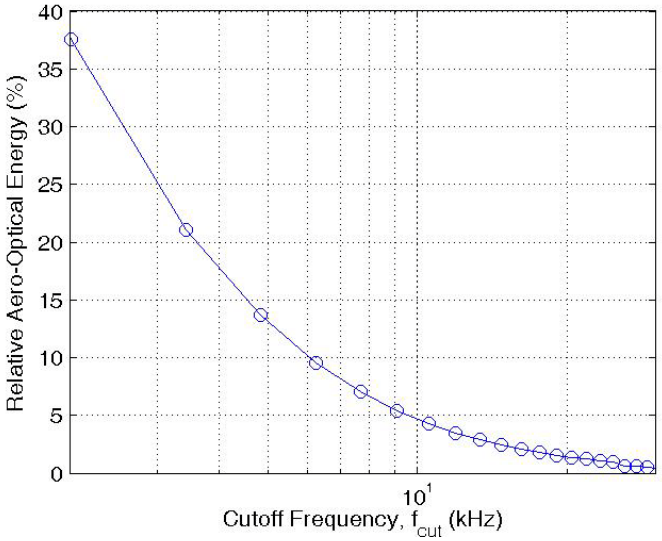

Figure 17: Relative amount of high-frequency aero-optical energy $OPD^2_{rms}(HF)$ as a function of cutoff frequency.

IV. Conclusions

This paper has presented results obtained from an experimental study of subsonic, compressible boundary layers over small backward-facing steps. Distinct regions in the streamwise evolution of the flow were identified using an array of scaling parameters. The results of Malley Probe measurements were shown to be in good agreement with experimental velocity measurements, as well as with previous studies. Aero-optical distortions of the boundary layer were significantly increased by the separated flow downstream of the backward step and even sufficiently downstream from the back-step the levels of the aero-optical distortions never went back to the undistorted levels, but rather leveled at a higher value. Furthermore, it is demonstrated that all essential characteristics of the sub-shear

layer evolution, the separation, the re-attachment, and the boundary layer recovery regions can be successfully recovered using non-intrusive aero-optical measurements.

In addition, a simple estimation of the aero-optical contribution of the near wall region of the incoming boundary layer was presented, and the preliminary qualitative results demonstrated that the near-wall region of the subsonic, compressible turbulent boundary layer does not contribute largely to the overall optical aberrations from the boundary layer. This result agrees with previous aero-optical measurements in the boundary layer which suggest that most-optically active flow structures are located in the outer region of the boundary layer.

The short streamwise extent of recovery region in this study did not allow for the observation of full boundary layer recovery. Further work is proposed to investigate the flow further downstream in the boundary-layer recovery region. The study of the flow environment for larger step heights would also prove useful in further refining scaling relationships for the effects of optical propagation through regions downstream of backward-facing steps.

Acknowledgments

This work is supported in part by the Air Force Office of Scientific Research, Grant number FA9550-09-1-0449. The U.S. Government is authorized to reproduce and distribute reprints for governmental purposes notwithstanding any copyright notation thereon.

References

[1] Jumper, E.J., and Fitzgerald, E.J., "Recent Advances in Aero-Optics," *Progress in Aerospace Sciences*, 37, 299-339.

[2] Cress, J., Gordeyev, S., Post, M, and Jumper E.J., "Aero-Optical Measurements in a Turbulent, Subsonic Boundary Layer at Different Elevation Angles," AIAA-2008-4214.

[3] Cress, J., Gordeyev, S., and Jumper E.J., "Aero-Optical Measurements in a Heated, Subsonic, Turbulent Boundary Layer," AIAA-2010-434.

[4] Cress, J. (2010) *Optical Aberrations Cause by Coherent Structures in a Subsonic, Compressible, Turbulent Boundary Layer*, PhD thesis, University of Notre Dame.

[5] Gordeyev, S., Duffin, D., and Jumper, E.J., "Aero-Optical Measurements Using Malley Probe and High-Bandwidth 2-D Wavefront Sensors," *International Conference on Advanced Optical Diagnostics in Fluids, Solids, and Combustion*, Tokyo, Japan, Dec. 2004.

[6] Armaly, B.F., Durst, F., Pereira, J.C.F., and Schönung, B., "Experimental and theoretical investigation of backward-facing step flow," *Journal of Fluid Mechanics*, Vol. **127**, 1983, pp 473-496.

[7] Le, H., Moin, P. and Kim, J., "Direct numerical simulation of turbulent flow over a backward-facing step," *Journal of Fluid Mechanics*, Vol. **330**, 1997, pp 349-374.

[8] Morris, S.C., and Foss, J.F.,E "Turbulent boundary layer to single-stream shear layer: the transition region," *Journal of Fluid Mechanics*, Vol. **494**, 2003, pp. 187-221.

[9] Minsuk, J., and Wang, M., "Sound generation by turbulent boundary-layer flow over small steps," *Journal of Fluid Mechanics*, Vol. 654, 2010, pp.161-193.

[10] Siegel, S., Seidel, J., and McLaughlin, T., (2009). "Experimental Study of Aero-Optical Distortions in a Free Shear Layer," AIAA-2009-361.

[11] Siegel, S., Seidel, J., and McLaughlin, T., (2009). "Transient forcing of a free shear layer: Experiments,", AIAA-2009-4297.

[12] D. Wittich, S. Gordeyev and E. Jumper, **"**Revised Scaling of Optical Distortions Caused by Compressible, Subsonic Turbulent Boundary Layers**"**, AIAA Paper 2007-4009.

[13] S. Gordeyev, E. Jumper and Hayden,T., "Aero-Optics of Supersonic Boundary Layers," AIAA Paper 2011-1325.